CALPHAD: Computer Coupling of Phase Diagrams and Thermochemistry 44 (2014) 70–80

Contents lists available at ScienceDirect

CALPHAD: Computer Coupling of Phase Diagrams and Thermochemistry

journal homepage: www.elsevier.com/locate/calphad

Ordering phase relationships in ternary iron aluminides

Luiz T.F. Eleno [a], Leonardo A. Errico [b,c], Pablo G. Gonzales-Ormeño [d], Helena M. Petrilli [a], Cláudio G. Schön [e,*]

[a] Instituto de Física, Universidade de São Paulo, CP 66318, 05315-970 São Paulo-SP, Brazil
[b] Departamento de Física and Instituto de Física La Plata (IFLP, CONICET-UNLP), Facultad de Ciencias Exactas, Universidad Nacional de La Plata, CC 67, 1900 La Plata, Argentina
[c] Universidad Nacional del Noroeste de la Provincia de Buenos Aires (UNNOBA), Monteagudo 2772, Pergamino, CP 2700 Buenos Aires, Argentina
[d] Universidad Nacional Tecnológica del Cono Sur de Lima, Sector 3, Grupo 1A 03 - Cercado, Villa El Salvador, Lima, Peru
[e] Computational Materials Science Laboratory, Department of Metallurgical and Materials Engineering, Escola Politécnica da Universidade de São Paulo, Av. Prof. Mello Moraes, 2463, CEP 05509—900 São Paulo-SP, Brazil

ARTICLE INFO

Available online 3 August 2013

Keywords:
First principles calculation
Cluster variation method
Order–disorder equilibria
Iron aluminides
Diffusion
Antiphase boundary energies

ABSTRACT

One of the key issues in the development of iron aluminides is the thermodynamic modeling of alloying effects on the long-range and short-range order states of the underlying bcc phase, needed for the proper description of their effects upon phase equilibria and physical properties of multicomponent alloys. The present work describes results obtained by the present research group in the development of a thermodynamic database using the cluster variation method (CVM) in the irregular tetrahedron approximation, combined with ab initio results obtained from FP-LAPW electronic structure calculation in the GGA approximation, as embodied in the WIEN2k package. The ordering phase equilibria in isothermal sections of systems Fe–Al–Mo, Fe–Al–Nb and Fe–Al–Ti are compared. These equilibria, particularly in the technologically important iron-rich corner, are characterized by radically different behaviors, ranging from very large solubility of Ti in the $L2_1/D0_3$ and B2 phases, to a very small solubility of Mo. The behavior of Nb is somewhat intermediate between these two extremes, and shows a limited solubility in the B2 phase, which is, however, found in metastable equilibrium with a $L2_1$ phase. It can be shown that these different behaviors can be understood as a consequence of the different metastable equilibria in the binary Fe–Mo, Fe–Nb and Fe–Ti systems. The results are discussed in reference with experimental data on the stable and metastable ordering equilibria in these systems and are illustrated by their impact of aluminide physical properties, like diffusion and APB energies, with its implications for plastic deformation.

1. Introduction

Iron aluminides, as technological materials, are multicomponent alloys, which, besides iron and aluminum, typically contain varying amounts of Cr, B, C, Mo, Nb, Ti, Zr, among others, as alloying elements [1–3]. While chromium and boron are added mainly to control and minimize the phenomenon known as "environmental embrittlement" [4,5], the remaining alloying additions aim at increasing strength by means of different mechanisms, like solid solution, precipitate and long-range or short-range ordering strengthening [2].

The control of these strengthening mechanism for an eventual alloy project relies, deeply, in the knowledge of the respective phase diagrams. The experimental approach has been employed and a great deal of information is known about the equilibria in the ternary Fe–Al–*M* (*M*=Cr, Mo, Nb, Ti, Zr) systems [2]. It happens that the phase equilibria in the region of interest (the iron-rich corner, involving the body centered cubic disordered solid solution, A2, or its ordered superlattices, the B2, $D0_3$ and $L2_1$ phases) varies considerably among these systems. For example, comparing the Fe–Al–Ti and Fe–Al–Mo systems, we observe that in the first system the $L2_1$ superlattice dissolves up to 20 at% Ti at 800 °C without precipitating more complex intermetallics [6,7], while in Fe–Al–Mo the maximum Mo solubility in the bcc ordered superlattice at 800 °C is about 5 at% [8].

In a previous work by some of the present authors these differences were traced back to the different equilibria observed in the stable or metastable binary bcc equilibrium in the Fe–*M* systems: Fe–Ti has a stable B2 phase at the center of the phase

* Corresponding author. Tel.: +55 113 091 5726; fax: +55 113 091 5243.
E-mail addresses: luizeleno@usp.br (L.T.F. Eleno), errico@fisica.unlp.edu.ar (L.A. Errico), pgonzales@untecs.edu.pe (P.G. Gonzales-Ormeño), hmpetril@if.usp.br (H.M. Petrilli), schoen@usp.br, claudio.schon@poli.usp.br (C.G. Schön).

0364-5916/$ - see front matter © 2013 Elsevier Ltd. All rights reserved.
http://dx.doi.org/10.1016/j.calphad.2013.06.009

diagram, while Fe–Mo has a miscibility gap, no ordered bcc superlattices being observed, not even as metastable phases [9]. The aim of the present work is to test this hypothesis by analyzing also the metastable equilibria in bcc Fe–Al–Nb system, which can be considered as an intermediate case in relation to Fe–Al–Mo and Fe–Al–Ti. The equilibria in the three systems will be compared and the results will be checked against available experimental results on metastable equilibria involving the $L2_1$ in Fe–Al–Nb [10].

Next, the impact of the different equilibria will be discussed in connection with two important non-equilibrium processes: ternary diffusion and antiphase boundary (APB) energies, with its implications to superdislocation properties and, hence, to plastic deformation.

2. Methodology

The procedure used for the phase diagram calculation is based on the so-called cluster expansion method [11]. In this approach, the total energies at the ground state ($T=0$ K) of a set of stoichiometric ordered compounds (which are related to a common disordered lattice) are calculated by solving one-particle Schrödinger equations. This set forms an orthonormal basis for the truncated expansion of the internal energy of the lattice at all temperatures and compositions, which are then used in conjunction with a statistical mechanics method to calculate the phase diagram.

The set used in the present work is defined by the adopted approximation, the irregular tetrahedron cluster, which corresponds to the unary disordered bcc compounds A2, the binary ordered B2, $D0_3$ and B32 compounds and the ternary ordered $L2_1$ and $F4\bar{3}m$ compounds.[1] This choice of basis is not unique and other approaches are found in the literature. Ghosh et al. [12], for example, used 38 compounds to model the bcc phase in the Hf–Nb system, and, more recently, Ravi et al. [13] used a unspecified, but very large, number of compounds to model the V–Nb, V–Ta and Nb–Ta systems. The basis set is kept limited here on purpose since only a simplified thermodynamic description of the thermodynamic properties of the bcc solid solution is sought. In addition, the adopted ground states are highly symmetrical, such that no relaxation of internal parameters are needed, and the compounds were optimized only through their lattice parameters. Other less symmetric ground states could, perhaps, be more stable than the ones adopted here, but they are not included in the present calculation since this would go beyond the scope of the chosen approximation: a thermodynamic description of the bcc phase, including its main ordered states, in the spirit of the CALPHAD method.

The total energies of the ordered compounds have been calculated using the WIEN2K code [14] in the framework of the Kohn–Sham scheme of the density functional theory (DFT), using the full potential-linearized augmented plane waves (FP-LAPW) method. The equilibrium lattice constants at the ground state have been determined through the calculation of the minimum value of the total energy. The self-consistent process has been performed until the difference of total energies per unit cell was smaller than 10^{-6} Ry in two subsequent calculations (1 Ry = 13.605698 eV). The standard procedure used here to achieve self consistency was already described in Ref. [15]. Exchange and correlation effects were treated with the generalized gradient approximation (GGA), using the implementations proposed by Perdew et al. [16]. All calculations were performed with the non-relativistic code, for compatibility with previously published results. A recent work by some of the present authors [15] suggests that the particular settings of the ab initio calculation (like the introduction of relativistic corrections) do have an impact on the obtained formation energies, but that phase diagram topology, in particular, is not affected.

The procedure used here is equivalent to the one employed in a previous work [9]. For easy reference, we rewrite the main equations for the present context. The calculated total energies for compound Φ (with Φ = B2, B32, $D0_3$, $L2_1$ or $F4\bar{3}m$) with $Fe_xAl_yM_z$ stoichiometry (where $n=x+y+z$ is the number of atoms in the unity formula and M=Ti, Nb, Mo) are denoted by $U^{\Phi}_{Fe_xAl_yM_z}$. These can be converted into formation energies, $\Delta^f U^{\Phi}_{Fe_xAl_yM_z}$, per mol of atoms in the reference state of the mechanical mixture of the components (with bcc structure), using

$$\Delta^f U^{\Phi}_{Fe_xAl_yM_z} = \frac{U^{\Phi}_{Fe_xAl_yM_z} - xU^{A2}_{Fe} - yU^{A2}_{Al} - zU^{A2}_{M}}{n} \quad (1)$$

As the A2 structure of iron is known to be ferromagnetic, all iron-containing compounds were calculated allowing for spin polarization. The calculated formation energies correspond, therefore, to magnetically ordered compounds in some of the cases.

The formation energies of the calculated compounds are used as input parameters to the cluster variation method (CVM), the statistical mechanics formalism adopted for the calculation of the phase diagrams. The CVM was first proposed by Kikuchi [17,18] as a method to derive entropy expressions for arbitrary lattices in arbitrary approximations. Later it was recognized that the CVM furnishes a standard procedure to derive factorizable partition functions of lattice systems within the mean-field approach [11]. The central concept of the CVM is the "basic cluster", which corresponds to a geometric figure contained in the reference lattice (not necessarily restricted to lattice points, see [19]) which represents the range of correlation lengths explicitly considered in the approximation. In the present work the irregular tetrahedron (IT) cluster approximation for the bcc lattice has been employed and is shown schematically in Fig. 1. The CVM formalism in the IT cluster approximation has been thoroughly outlined in several previous publications by the present group [20,21,9] and therefore only the aspects which are relevant to the discussion of the results will be reproduced here.

The internal energy (U) of a bcc lattice with N sites (containing $6N$ irregular tetrahedra) is written as [22]

$$U = 6N \sum_{i,j,k,l\,=\,\mathrm{Fe,Al},M} \varepsilon^{\alpha\beta\gamma\delta}_{i,j,k,l} \rho^{\alpha\beta\gamma\delta}_{i,j,k,l}. \quad (2)$$

In this expression, $\rho^{\alpha\beta\gamma\delta}_{ijkl}$ represents the probability of finding an $\{\alpha\beta\gamma\delta\}$ IT cluster with configuration $\{ijkl\}$ (i.e., species i occupying cluster position α, j in cluster position β and so on) out of the $6N$ tetrahedra which correspond to the system and $\varepsilon^{\alpha\beta\gamma\delta}_{ijkl}$ represents the eigenenergy associated with this configuration. The stoichiometric compounds at the ground state correspond to particular configurations: a B2 FeNb stoichiometric compound with N lattice points, for example, may be built by $6N$ tetrahedra with configuration FeFeNbNb, while the B32 FeNb, $D0_3$ Fe_3Nb and $FeNb_3$ stoichiometric compounds are similarly obtained using the FeNbFeNb, FeFeFeNb and FeNbNbNb configurations. Eq. (2) may be now applied to these

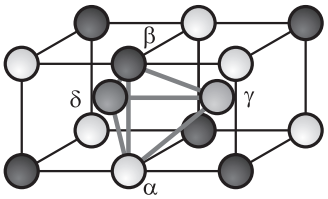

Fig. 1. The irregular tetrahedron (IT) cluster in the bcc lattice.

[1] The "$F4\bar{3}m$ structure" corresponds to the prototype $CuHg_2Ti$ and has no Strukturbericht designation; we therefore decided to represent this compound by its space group symbol.

particular cases and the compound formation energies are associated with the corresponding cluster eigenenergies. In the case of the B2 FeNb compound, for example

$$\varepsilon^{\alpha\beta\gamma\delta}_{\mathrm{Fe,Fe,Nb,Nb}} = \frac{\Delta^f U^{B2}_{\mathrm{FeNb}}}{6N} \tag{3}$$

It must to be reminded that the eigenenergy matrix $\{\varepsilon^{\alpha\beta\gamma\delta}_{i,j,k,l}\}$ is highly degenerate due to symmetry constraints imposed by the crystal lattice. Both configurations FeNbFeNb and NbFeNbFe, for example, represent a B32 FeNb stoichiometric compound, differing only by a translation of the origin of the lattice by the vector $a_0/2[1\ 1\ 1]$ (where a_0 represents the lattice constant of the B32 structure). Since the energy of a compound cannot depend on the choice of the origin, it follows that $\varepsilon^{\alpha\beta\gamma\delta}_{\mathrm{Fe,Nb,Fe,Nb}} = \varepsilon^{\alpha\beta\gamma\delta}_{\mathrm{Nb,Fe,Nb,Fe}}$. The same is true for the two remaining degenerate configurations FeNbNbFe and NbFeFeNb.

The set $\{\varepsilon^{\alpha\beta\gamma\delta}_{ijkl}\}$, including the three reference values, $\varepsilon^{\alpha\beta\gamma\delta}_{M,M,M,M} = \varepsilon^{\alpha\beta\gamma\delta}_{\mathrm{Fe,Fe,Fe,Fe}} = \varepsilon^{\alpha\beta\gamma\delta}_{\mathrm{Al,Al,Al,Al}} = 0$, contains all information needed for the description of the system. It is a common practice in the literature, however, to further decompose the configuration eigenenergies into pair contributions (nearest and next-nearest neighbors), completing the set with other cluster interactions (see e.g., [22,23]). This will not be done in the present work, since the results are better appreciated using directly the compound formation energies instead.

2.1. Cluster variation method (CVM) calculations

With the definition of the internal energy, Eq. (2), we may build the free energy, F, of the system as

$$F = U - TS - \sum_{i,j,k,l\,=\,\mathrm{Fe,Al},M} \frac{\mu^*_i + \mu^*_j + \mu^*_k + \mu^*_l}{4} \rho^{\alpha\beta\gamma\delta}_{i,j,k,l} \tag{4}$$

In this expression, S stands for the configurational entropy of a bcc lattice in the irregular tetrahedron cluster approximation, which is found, e.g., in Ref. [24]. Variable μ^*_i represents the chemical potential of component i in the "baricentric" reference state, defined by condition

$$\mu^*_i = \mu_i - \frac{1}{3}\left(\mu_{\mathrm{Fe}} + \mu_{\mathrm{Al}} + \mu_M\right) \Rightarrow \sum_{j\,=\,\mathrm{Fe,Al},M} \mu^*_j = 0 \tag{5}$$

where μ_{Fe}, μ_{Al} and μ_M are the chemical potentials of iron, aluminum and M=(Mo,Ti,Nb) in any reference state (e.g., the standard element reference, SER [25]). Using the identity [26]

$$U - TS = N \sum_{i\,=\,\mathrm{Fe,Al},M} \mu_i x_i \tag{6}$$

and substituting it, with (5), into (4), we obtain

$$F = N\left(\frac{\mu_{\mathrm{Fe}} + \mu_{\mathrm{Al}} + \mu_M}{3}\right) \tag{7}$$

Using Eq. (5) and solving for the chemical potential of component i, we obtain

$$\mu_i = F + \mu^*_i \tag{8}$$

Eq. (4) is minimized using a specific algorithm called "natural iteration method" (NIM) [27]. The NIM is a numerical self-consistent iterative algorithm and, therefore, requires the setting of a convergence criterion. In the present work the convergence condition to reach a stable or metastable configuration was set to a difference smaller than $10^{-4}\ k_B$ units ($\approx 10^{-3}$ J mol^{-1}; k_B is Boltzmann constant) between two values of F obtained in subsequent iterations of the NIM. For given values of T and $\{\mu^*_{\mathrm{Al}}, \mu^*_M\}$ one may eventually obtain different solutions for the minimum (either global or local) of F using suitable choices of initial conditions. Whenever the algorithm converges to different phases (say, λ and ξ), the equilibrium condition will be given by

$$F^{\lambda}|_{T,\mu^*_{\mathrm{Al}},\mu^*_M} = F^{\xi}|_{T,\mu^*_{\mathrm{Al}},\mu^*_M} \tag{9}$$

A calculation of an isothermal section of a ternary phase diagram corresponds to mapping all possible solutions of Eq. (9) as functions of μ^*_{Al} and μ^*_M, for all pairs of stable configurations, λ and ξ, at a given temperature T. As it was already discussed by some of us in a previous publication [21], although the topology of the calculated phase diagrams is expected to be well reproduced, the approach used in this work is known to lead to significant overestimation of the temperature scale in many intermetallic systems (see e.g., Ref. [28]) and, as a consequence, the transition temperatures and phase boundary compositions may differ significantly from the experimental data. The disagreement can be attributed either to the fact that we ignore relevant thermodynamic degrees of freedom [29] and the different approximations involved in our calculations (for example, contributions to the free energy originated from magnetic and vibrational entropy were not taken into account), or to a lack of convergence of the cluster expansion [30]. These approximations are necessary due to the complexity of the system under study. It is also well-known that DFT may present problems in the description of Fe–Al alloys [21,31,32]. However, the main features and the qualitative trends of the metastable phase diagrams are reproduced correctly, providing useful insights and important physical information on iron aluminides.

2.2. Impact of thermodynamics on the aluminide physical properties

Thermodynamics, although referring to equilibrium states, has an impact also over the physical properties (which usually are defined only in non-equilibrium situations) of the corresponding aluminides. Below we address two important non-equilibrium processes:

1. Ternary diffusion.
2. Antiphase boundary (APB) energies, leading to superdislocation geometry.

As stated in Ref. [33], the impact of thermodynamics in diffusion in ternary ordering systems is well represented by a simple substitutional atom exchange diffusion model. Although it is well known that diffusion in metallic alloys (including superlattices) is vacancy-mediated, this simple model allows a better appreciation of the effects of second-order boundaries and stoichiometric lines without the complexity of introducing vacancies in the thermodynamic model. This model is representative, however, since the vacancy concentration in alloys is usually very small, always close to the limit of infinite dilution, so Raoult's law holds.[2]

According to the simple exchange model, in the linear regimen of irreversible thermodynamics [34] the atom fluxes of the three components, $\vec{j}_i$, are coupled due to the mass balance condition, leading to the generalized phenomenological law

$$\vec{j}_i = -\sum_k M_{i,k} \vec{\nabla}(\mu_k - \mu_{\mathrm{Fe}}) \quad (i,k = \mathrm{Al,M}) \tag{10}$$

where $M_{i,j}$ represent the species' mobilities and μ_j represent the j species' chemical potential. Functions $\phi = (\mu_{\mathrm{Al}} - \mu_{\mathrm{Fe}})$ and $\rho = (\mu_{\mathrm{M}} - \mu_{\mathrm{Fe}})$ act, therefore, as generalized thermodynamic forces for diffusion. In binary diffusion it is usual to express this as a

[2] Raoult's law states that in the limit of infinite dilution the solvent (that is, the alloy) behaves as an ideal solution, regardless of the diluted species (in the present case, the vacancies) [26]. In other words, the activities of the elements in the alloy are only marginally affected by the presence of vacancies.

multiplicative factor which is added to the conventional Fick's law.[3] This multiplicative factor is called the "thermodynamic factor for diffusion". As one of the present authors showed, this factor present discontinuities across second-order boundaries and maxima associated to stoichiometric compositions of superlattices [36]. In principle, in the case of ternary diffusion, a similar transformation could be performed but, instead, here we use directly the functions ϕ and ρ, as suggested in Ref. [33].

The second case discussed here refers to the calculation of antiphase boundary (APB) energies. APBs are planar defects intrinsic of superlattices and are characterized by a discontinuity in the distribution of species among the crystal sublattices. APBs are the superlattice equivalents of magnetic domain walls in antiferromagnetic crystals. In iron aluminides, APBs are potentially formed by two processes.

In the first process, APBs may be formed in the course of the transition from the disordered to the ordered structure, i.e., whenever a second-order boundary is crossed during cooling. By this process different parts of the disordered crystal start ordering by a local symmetry break wave which forms a partition of the original lattice into sublattices, with different site occupancies. Two different and uncorrelated regions, hence, start growing by propagation of this perturbation and when they impinge in each other, this preferential occupation may not agree in both sides of the interface. The formed defect (the interface) is an APB. By its own nature, this defect forms in conditions where short-range diffusion is fast, hence, it forms under local equilibrium. This kind of defect is referred to as a "thermal" APB. Its free energy may be calculated using the CVM in two different methods: the "sum" method (S-CVM) [37] and the "scalar product" method (SP-CVM) [38,39].

APBs, however, may also be formed as a consequence of dislocation slip. A dislocation produces a displacement of one part of a crystal relative to the other across the slip plane, hence, it may disturb the superlattice order producing an APB. Contrary to thermal APBs, however, these defects may be formed under conditions in which short-range diffusion is suppressed or delayed (for example, by cold working). This kind of defect is referred to as a "mechanical" APBs and they are modeled by setting boundary conditions corresponding to the equilibrium correlations observed in the perfect crystal in thermodynamic equilibrium, except across the defect plane. The standard method to calculate the energy of such defects is to count the correlations which are broken by the passage of the dislocation, subtracting them from the bonds which are reformed by the process [40]. This method is referred as the bond-counting (BC) method and has been applied by one of the present authors to the irregular tetrahedron approximation of the CVM in bcc lattices [41,42]. This formalism will be employed in the present work.

3. Results and discussion

3.1. Electronic structure calculations

The rather extensive list of compounds needed for a complete assessment of three ternary systems in the irregular tetrahedron approximation can be reduced by observing that many of the corresponding subsystems have already been investigated by the present authors in previously published works, namely, the Mo–Al [9,20], the Fe–Al [21] the Fe–Ti [43], and the Fe–Mo and Fe–Al–Mo [9,15] systems. These results will not be reproduced here and the reader is referred to the original works for details on the results of the electronic structure calculations for these systems. The remaining systems will be described in what follows. Table 1 shows the results of the electronic structure calculations for the compounds of the investigated systems.

Direct interpretation of Table 1 is not trivial. A conclusion about stability of compounds in the ground state of the respective systems depends on the determination of the so-called "convex hull". For example, the B2 phase in system Fe–Nb, in spite of showing a negative formation enthalpy, will not be stable in the ground state since its formation energy is less negative than the one corresponding to a heterogeneous state formed by the $D0_3$-Fe_3Nb and the A2-Nb phases at $x_{Nb} = 0.5$. Analysis of the stability on ternary compounds is even more complex, since the convex hull corresponds to a set of planes, but both systems show larger stabilities for the $L2_1$-Fe_2AlM and $F4\bar{3}m$–Al_2FeM compounds, while compounds close to the stoichiometry M_2AlFe in either structures have mixed tendencies, but with smaller formation energies. This same behavior is observed in system Fe–Al–Mo [9], pointing out to a trend in the ternary transition metal iron aluminides.

The present results agree well with independent results obtained by Alonso et al. [44]. Small differences in the compound formation energies may be attributed either to the use of different electronic structure calculation methods or to the inclusion of relativistic corrections. Qualitatively, however, the compound stability sequence observed by Alonso et al. [44] for systems Fe–Al–Ti and Fe–Al–Nb agrees with the present results.

Comparison with experimental values is only possible for the $L2_1$-Fe_2AlTi compound. Palm et al. [6] report a room temperature lattice parameter value for a $D0_3$ phase containing 25 at% Ti (i.e., the $L2_1$ compound) previously annealed at 1000 °C (1273 K) and

Table 1
Results of the electronic structure calculations for the compounds of systems Fe–Al–*M* (*M*=Ti,Nb) performed using the FP-LAPW method (Wien2k code). Lattice parameters (a_0) are expressed in nanometers. Formation energies are given in kJ mol^{-1}.

Compound	Structure	a_0	$\Delta^f U^\Phi$
Fe	A2	0.286	0.0
Ti	A2	0.326	0.0
Nb	A2	0.332	0.0
Mo	A2	0.318	0.0
Al	A2	0.324	0.0
FeNb	B2	0.308	−0.788
Fe_3Nb	$D0_3$	0.593	−3.774
FeNb	B32	0.615	+6.892
$FeNb_3$	$D0_3$	0.638	+2.691
TiAl	B2	0.319	−36.888
Ti_3Al	$D0_3$	0.647	−26.583
TiAl	B32	0.641	−20.577
$TiAl_3$	$D0_3$	0.640	−7.417
NbAl	B2	0.324	−10.896
Nb_3Al	$D0_3$	0.658	−10.502
NbAl	B32	0.647	−15.097
$NbAl_3$	$D0_3$	0.642	+4.627
Fe_2AlTi	$L2_1$	0.579	−48.079
Fe_2AlTi	$F4\bar{3}m$	0.585	−25.535
Al_2TiFe	$L2_1$	0.601	−27.534
Al_2TiFe	$F4\bar{3}m$	0.598	−43.157
Ti_2FeAl	$L2_1$	0.614	−33.869
Ti_2FeAl	$F4\bar{3}m$	0.608	−30.456
Fe_2AlNb	$L2_1$	0.592	−36.462
Fe_2AlNb	$F4\bar{3}m$	0.609	−10.502
Al_2NbFe	$L2_1$	0.620	−12.307
Al_2NbFe	$F4\bar{3}m$	0.617	−22.711
Nb_2FeAl	$L2_1$	0.632	−3.873
Nb_2FeAl	$F4\bar{3}m$	0.632	−1.838

[3] Which expresses the diffusion fluxes as a function of concentration gradients instead of the gradient of the chemical potentials [35].

quenched in water thereafter. The reported value corresponds to $a_0=0.5878$ nm. This result is in agreement with a more recent value by Yan et al. [45] for the stoichimetric compound after annealing at 900 °C (1173 K) followed by water quenching, which corresponds to $a_0=0.58813$ nm. Both values are consistent with the present calculation. The small difference may be attributed either to lattice expansion from the ground state to room temperature or to minor uncertainties intrinsic to the electronic structure calculations in the framework of the Kohn–Sham scheme of the DFT.

3.2. Phase equilibria

3.2.1. Binary systems

Fig. 2 shows the calculated phase diagrams for the binary systems with iron. A central point of the present work relies on the different topologies of the Fe–M (M=Mo,Nb,Ti) phase diagrams. In particular the Fe–Ti and Fe–Mo systems show radically different topologies. In the first case the system is dominated by a central field of stability of the B2 phase. This phase is observed as a stable phase in the experimental Fe–Ti phase diagram [46,47]. The formation energy of the B2-FeTi phase amounts -48 kJ mol^{-1} [43], which is substantially larger than the formation energy of the B2-FeAl phase (-36 kJ mol^{-1}) [48]. The Fe–Mo system, on the contrary, shows a miscibility gap, so no ordered bcc compound, based on the irregular tetrahedron approximation, is even predicted to be metastable in this system. The experimental Fe–Mo phase diagram presents, however, other stable phases with more complex structures (for example, the $\mu-Fe_7Mo_6$, phase). A thermodynamic assessment of the system shows that the mixing enthalpy of Fe and Mo in the bcc phase is positive [49], showing that a metastable miscibility gap in the bcc phase is indeed expected for this system, although it cannot be experimentally observed. A simple thermodynamic calculation using this model, but suppressing all intermetallic phases result in a miscibility gap which is qualitatively in agreement with the one shown in Fig. 2b. The Fe–Nb system corresponds to an intermediate case between both limits. This system shows both a miscibility gap (at the Nb-rich side) and metastable ordered compounds (at the Fe-rich side). In the Fe–Nb system, demixing and ordering occur at considerably lower temperatures than in the other Fe containing systems.

Fig. 3 shows the metastable phase diagram of the aluminum-containing binary systems. As in the previous cases, all three systems present different topologies. In the present cases, however, the differences are less significant. For example, all three systems present an ordered compound at the AlM stoichiometry: a B2 phase in the case of Al–Ti and a B32 compounds in Nb–Al and Mo–Al. In addition, the Al–Ti and Al–Nb systems show stable $D0_3$ phases at the transition metal-rich side, while Mo–Al shows a heterogeneous state composed by A2-Fe and B32-AlMo in the same region. Similar to Fe–Nb, the temperature scale of the Al–Nb phase diagram is considerably lower than the others. Concerning the experimental phase diagrams, the observed ζ_2 phase in the Al–Mo phase diagram [50], close to the equiatomic composition, could actually correspond to a B32 structure, as we have discussed in a previous publication [20]. The Al–Ti system shows a small region of stability of the B2-AlTi phase in the region $0.3\lesssim x_{Al}\lesssim 0.44$ and 1473 K$\lesssim T\lesssim$1623 K [51,52]. This result is consistent with the present calculations if the already mentioned overestimation of the temperature scale is taken into account. The case of system Al–Nb is more complex, since the bcc phase is stable only in a small region close to the Nb corner (up to $x_{Al}\approx 0.15$), so no ordered compound is expected to be experimentally observed. The most recent thermodynamic assessment of this system [53], however, suggests that interaction between Al and Nb in the bcc phase is small, but negative, at the Nb-rich side, so this assessment predicts ordering tendency in the bcc solid solution, but with low transition temperatures, which is consistent with our calculations.

3.2.2. Ternary systems

Fig. 4 shows three isothermal sections of the Fe–Al–Mo phase diagram, depicting the interaction of the miscibility gap which originated from the binary Mo–Fe phase diagram with the two phase fields involving the B2 and A2 phases. As explained in Ref. [9], this interaction limits the maximum Mo solubility in the B2 phase at

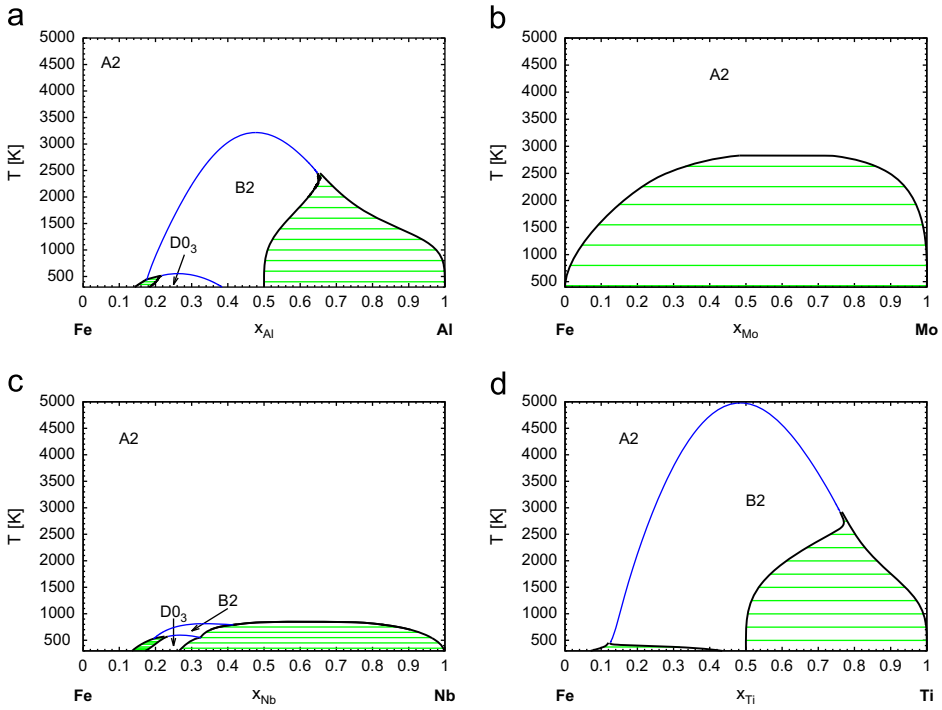

Fig. 2. Binary metastable bcc phase diagrams of the iron-containing systems: (a) Fe–Al [21], (b) Fe–Mo [9], (c) Fe–Nb, and (d) Fe–Ti [43].

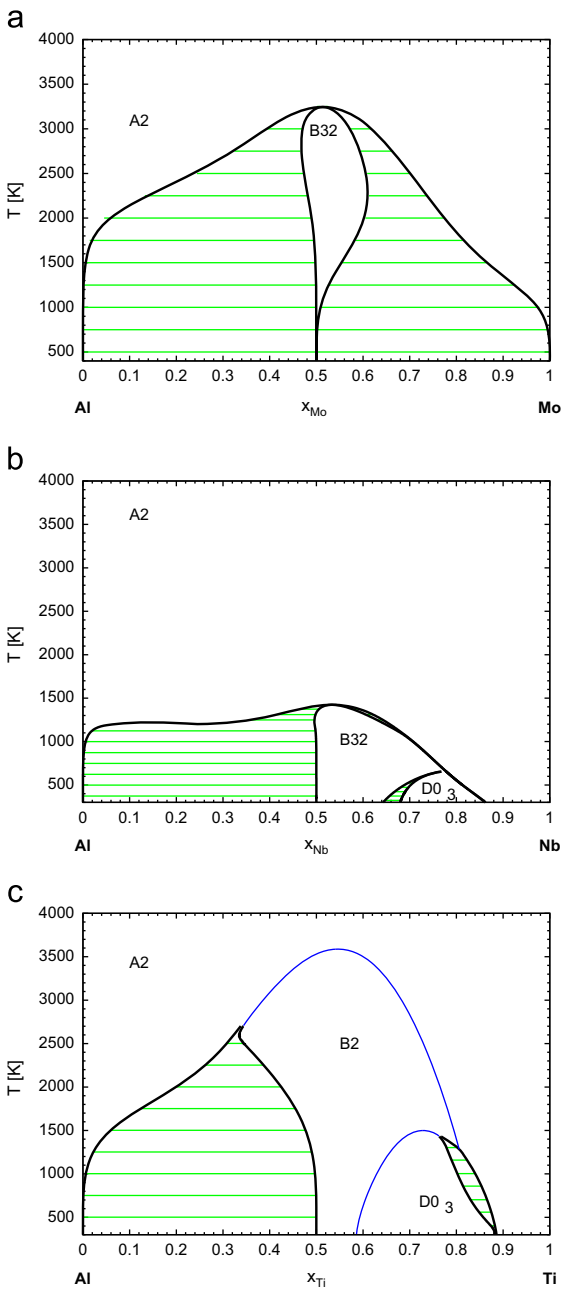

Fig. 3. Binary metastable bcc phase diagrams of the aluminum-containing systems: (a) Al–Mo [9], (b) Al–Nb, and (c) Al–Ti.

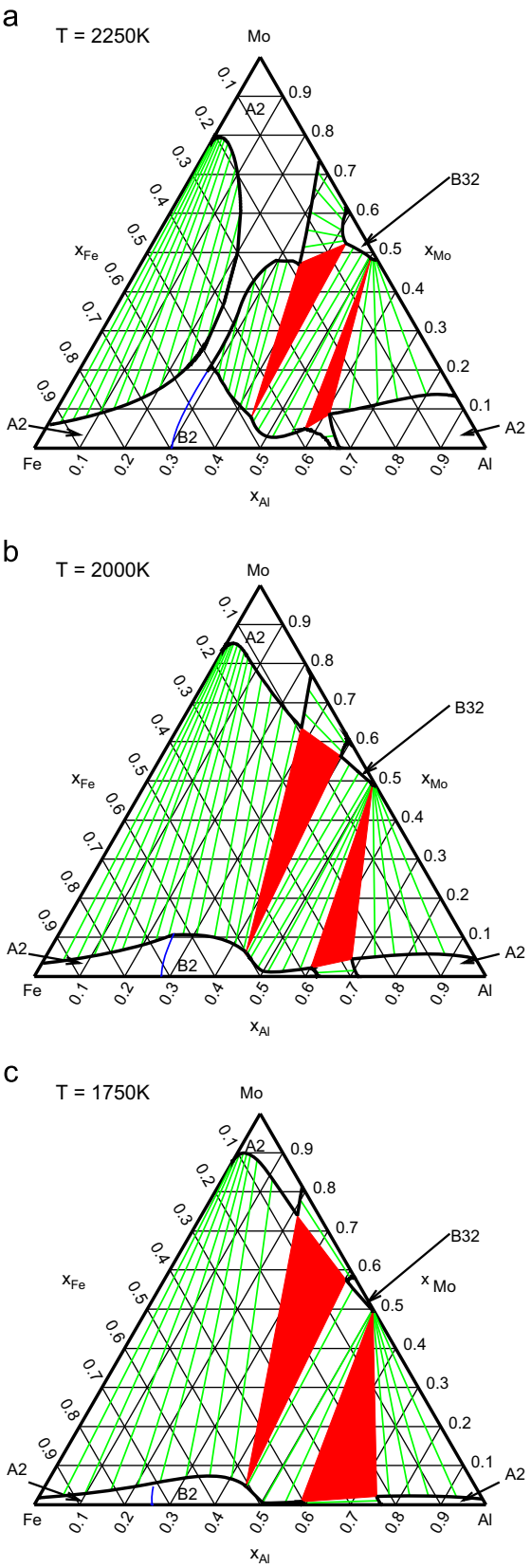

Fig. 4. Isothermal sections of the metastable bcc Fe–Al–Mo phase diagram: (a) at T=2250 K, (b) at T=2000 K, and (c) at T=1750 K [9].

low temperatures, justifying the sharp decrease in solubility experimentally observed [8,54].

Fig. 5 shows three isothermal sections of the metastable bcc Fe–Al–Ti system. In contrast with the Fe–Al–Mo system, this case shows a large field of homogeneous states corresponding to the disordered solid solution and to its ordered states stable up to very high titanium contents. This large field occupies the entire iron-rich corner and heterogeneous states are limited to a quite small two-phase field involving the $L2_1$ phase and the B2 phase. This topology is observed in the experimental phase diagram [7] and results in very large titanium solubilities in the $L2_1$ phase when in equilibrium with the Laves $(Fe,Al)_2Ti$ compound. The topology in the titanium-rich corner in the 2000 K isotherm (Fig. 5a) shows that the A2-Ti+B2-TiFe equilibria is, in fact, originated from a B2–B2′ miscibility gap in concentrated ternary alloys and not from a multicritical point in the A2-Ti/B2-TiAl second-order line, as predicted by the phenomenological CVM calculation (which was fitted to phase equilibria data in the iron-rich corner) shown by Ohnuma et al. [7]. This miscibility gap, however, is experimentally observed in the 1273 K

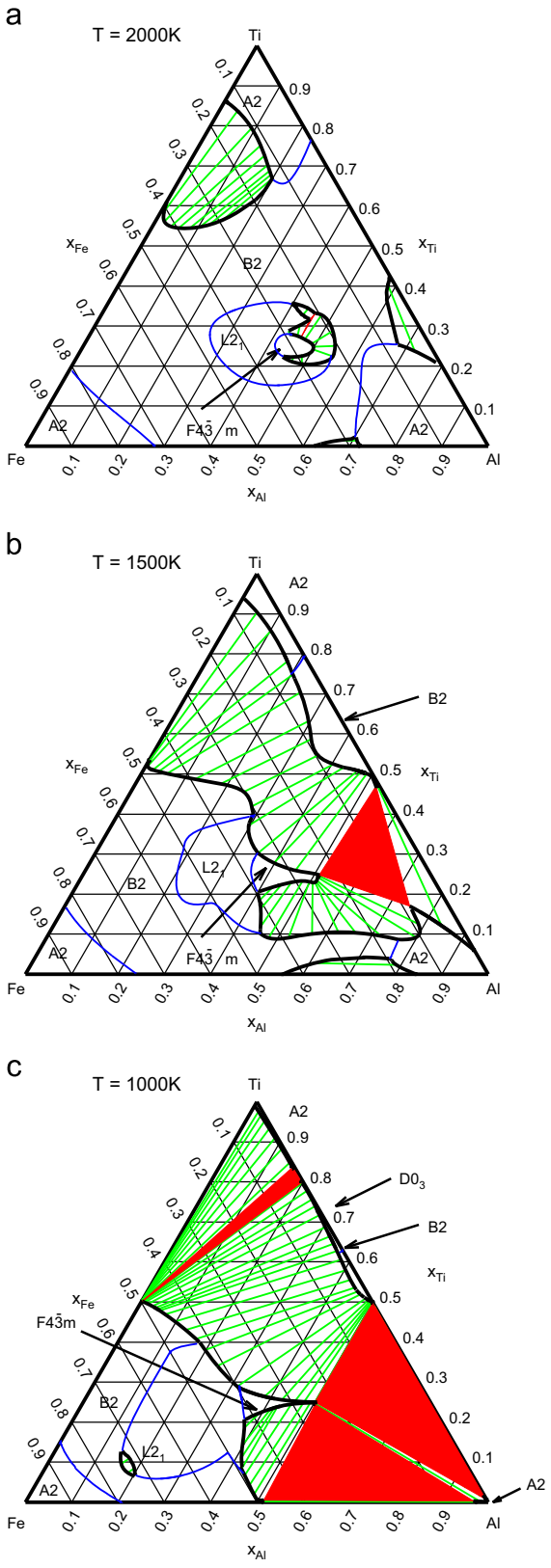

Fig. 5. Isothermal sections of the metastable bcc Fe–Al–Ti phase diagram: (a) at $T=2000$ K, (b) at $T=1500$ K, and (c) at $T=1000$ K.

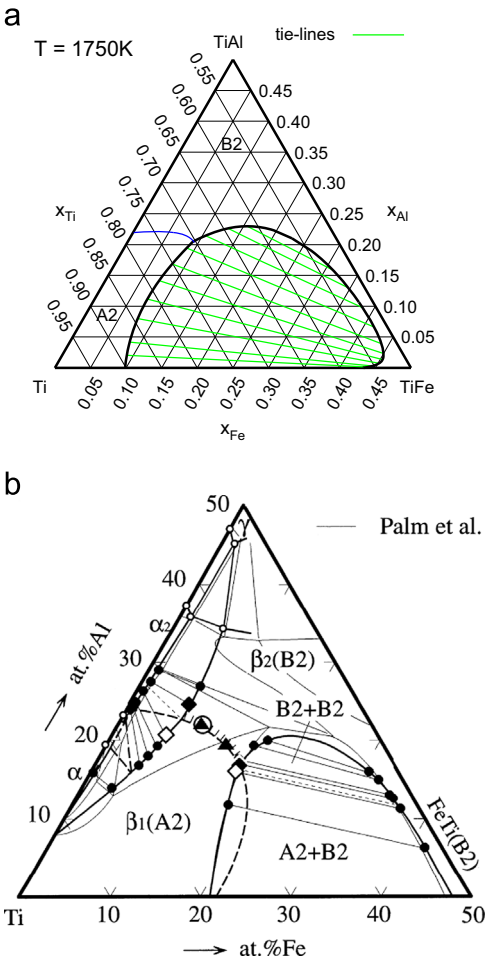

Fig. 6. Theoretical isothermal section of the metastable bcc Fe–Al–Ti phase diagram at 1750 K in the Ti-rich corner (a) and experimental section at 1273 K (b) [51] ("Palm et al." corresponds to Ref. [6] in the present work).

isotherm in the Ti–Al–Fe system [51]. This can be better seen using the additional isotherm at 1750 K shown in Fig. 6, which is limited to the Ti-rich corner to allow for direct comparison with Kainuma et al. [51] results. We notice that the comparison between isotherms at different temperatures was performed due to the fact that we expect to have an overestimated temperature scale. Similar miscibility gaps form in ternary B2 fields whenever the strong B2 phases are found in the three limiting binary systems, a feature which has been attributed (by two of the present authors) to frustrated states in the B2 structure [55].

Another relevant feature observed in the present calculations is the existence of a F43$\bar{}$m phase close to the Al_2FeTi stoichiometry (see Fig. 5). A stable phase at this stoichiometry, labeled T2, is indeed observed experimentally in the Fe–Al–Ti system [56]. This stable phase is found in equilibrium with the $L2_1$ and B2 superlattices and has cubic symmetry, but with a more complex crystal structure, which is labeled "G-phase" [57]. Although it is intriguing to find a complex ordered superlattice in the same region, the investigation of a close relationship between the crystal structure of the T2 phase and the F43$\bar{}$m superlattice is out of the scope of the present work.

Finally, Fig. 7 shows three isothermal sections of the metastable bcc Fe–Al–Nb system. As predicted, the phase diagram topology is intermediate between both previous cases. The A2 and B2 phases have a limited solubility of a third element, not extending far into the ternary. This is mainly due to the equilibrium with a quite stable $L2_1$ compound. The two phase fields (A2+$L2_1$ and B2+$L2_1$), therefore, are an expanded version of the one observed in Fe–Al–Ti (Fig. 5). Although the Nb solubility in the B2 phase close to the Fe–Al binary system is as low as observed in the case of system Fe–Al–Mo (Fig. 4), the nature of the heterogeneous equilibrium which limits this solubility is totally

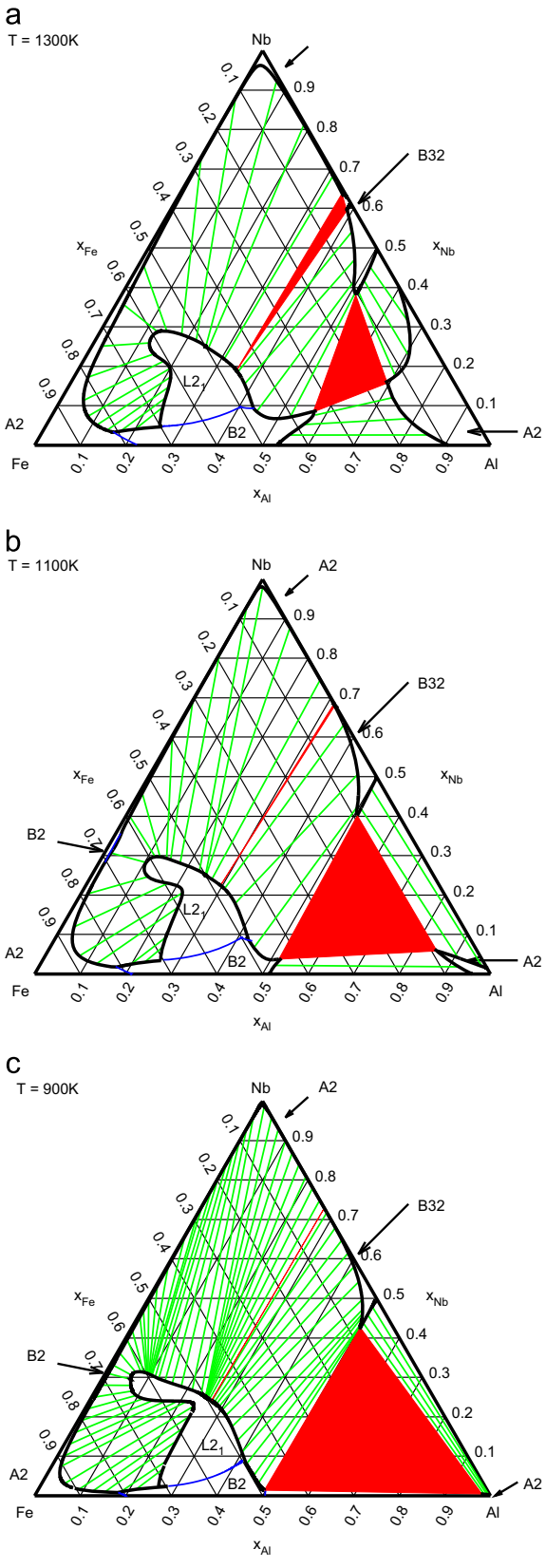

Fig. 7. Isothermal sections of the metastable bcc Fe–Al–Nb phase diagram: (a) at $T=1300$ K, (b) at 1100 K, and (c) at $T=900$ K.

different. In the case of Nb, the second phase in (metastable) equilibrium is also an aluminide and not a complex intermetallic, as the A15-Mo_3Al phase. It is interesting to observe that a metastable heterogeneous equilibrium between the $L2_1$ and the B2 phase has been experimentally observed in the Fe–Al–Nb system [10]. These authors observed needle-like transition precipitates of the Heusler phase in quenched and aged-hardened samples of alloys with 15–20 at% Al and 2–5 at% Nb. The needle-like morphology was attributed to a large difference in specific volume for both alloys, which points-out to a large difference in composition between both phases (close to the multicritical point, where the first-order equilibrium turns into a second-order transition, the difference in specific volume between the phases must vanish since the later transition is, by definition, continuous).

3.3. Isopotential lines

Fig. 8 shows a detail of the Fe–Al–Mo system in the stability region of the $D0_3$-Fe_3Al compound, in order to be able to do so, a smaller temperature (600 K) was selected. Superimposed to this section, the isopotential lines of ϕ and ρ (defined in Section 2.2) are plotted. Since only the differences $\Delta\phi$ and $\Delta\rho$ are physically relevant, no attempt was made to identify the values corresponding to each isopotential line. Instead, the lines are spaced such that this difference amounts 2.5 kJ mol^{-1} between two neighboring lines.

The first apparent feature in this figure is that the behavior of the isopotential lines (and hence, of the thermodynamic potential for diffusion in the ternary alloy) is markedly non-linear. Further, the slope of the lines is discontinuous at the $D0_3$/B2 second-order boundary. Similar discontinuities have been observed in a phenomenological calculation of system bcc Fe–Cr–Al [33], suggesting it should be a general feature of second-order boundaries.

The solution of a diffusion problem in a ternary system, of course, depends on many factors, including the set of boundary conditions and the composition dependence of the mobilities. The thermodynamic effect clearly shows, however, that straight diffusion paths are unlikely to be observed in systems which present configurational order. In particular, if the diffusion path crosses a composition corresponding to a second-order boundary, it will show a discontinuity in its slope. This kind of slope discontinuities in diffusion paths has been experimentally reported (e.g., [58,59]), and metallographically associated with the position of the boundary between the ordered and the disordered phases at the equilibration temperature (i.e., the second-order boundary).

Fig. 9 shows the region of stability of the ordered aluminides in system Fe–Al–Ti at the 1000 K isotherm, including the isopotential lines (which are spaced by a 5 kJ mol^{-1} difference). Due to the larger composition range in this figure, compared to the previous case, the behavior of the isopotential lines is also richer. In particular, a concentration of isopotential lines is observed along

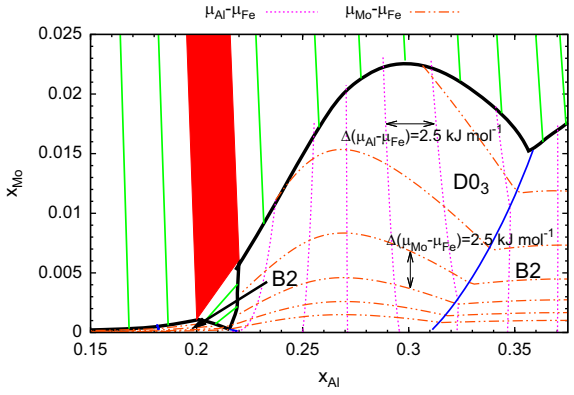

Fig. 8. Detail of the 600 K isothermal section of system Fe–Al–Mo in the stability region of the $D0_3$-Fe_3Al compound, showing the $\mu_{Al}-\mu_{Fe}$ and $\mu_{Mo}-\mu_{Fe}$ isopotential lines.

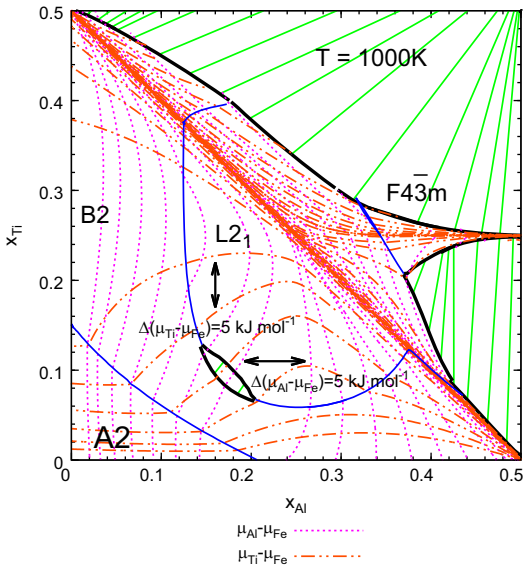

Fig. 9. Detail of the 1000 K isothermal section of system Fe–Al–Ti in the iron-rich region, showing the $\mu_{Al}-\mu_{Fe}$ and $\mu_{Ti}-\mu_{Fe}$ isopotential lines.

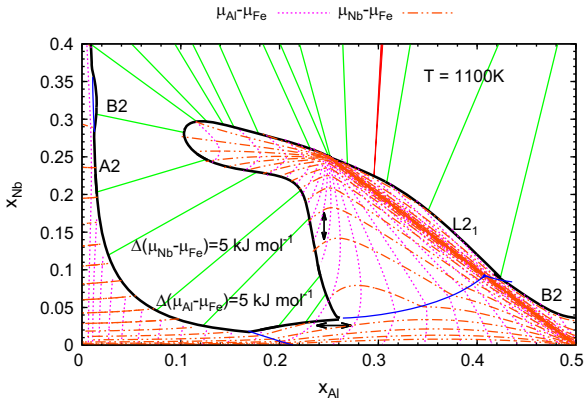

Fig. 10. Detail of the 1100 K isothermal section of system Fe–Al–Nb in the iron-rich region, showing the $\mu_{Al}-\mu_{Fe}$ and $\mu_{Nb}-\mu_{Fe}$ isopotential lines.

the section which joins the B2-FeAl and B2-FeTi compounds. This is the ternary equivalent of the maximum in the thermodynamic factor for diffusion observed at stoichiometric compositions in binary systems [36]. As in the case of Fe–Al–Mo, the behavior of the isopotential lines in the Fe–Al–Ti system is markedly non-linear and presents slope discontinuities in the second-order boundaries. It is interesting to notice that the isopotential lines can provide 'hints' about equilibria observed at lower temperatures. For example, the isopotential lines of the $\mu_{Ti}-\mu_{Fe}$ function seem to diverge when approaching the binary Fe–Ti side, close to $x_{Ti}=0.25$. This is an indication of the onset of the two-phase B2+A2 equilibria below ≈450 K (see Fig. 2d).

In order to complete the set, Fig. 10 shows a detail of the 1100 K isotherm in the Fe–Al–Nb system, in the region of stability of the $L2_1$ compound. The main features observed in the Fe–Al–Ti system are also observed in this section, but the strong concentration of isopotential lines at the $Fe(Nb_y, Al_{1-y})$ section is limited by the two-phase $L2_1$+A2 field, which coincides with the ideal stoichiometry of the $L2_1$ superlattice ($x_{Al}=0.25$ and $x_{Nb}=0.25$). However, contrary to Fe–Al–Ti, the isopotential lines seem to irradiate from this point, showing that the thermodynamic properties of the Heusler phase is fundamentally different in both systems.

3.4. APB energies

Plastic deformation by slip in superlattices takes place by propagation of the so-called "superdislocations", which correspond to ordinary dislocations decomposed into two, three or even four partial dislocations, bound by planar defects like stacking faults (SF), anti-phase boundaries (APBs) or combinations of both [60]. In the case of the bcc-based superlattices, superdislocations are composed of four-fold (for $D0_3$ and $L2_1$) or two-fold (for B2) aggregates of $a_0/2\langle 1\,1\,1\rangle$ partials slipping in $\{0\,1\,\bar{1}\}$ planes. These dislocations are mostly observed in near-screw orientations and each partial is bound to the group by APBs (in the case of $D0_3$ and $L2_1$, of two kinds) [42,61,62].

In the course of plastic deformation one of the components of the superdislocation may become immobilized, while the remaining ones continue to slip. This results in the growing of a ribbon of the corresponding plane defect (i.e., an APB), which contributes to the stored plastic deformation energy. The superdislocation may also interact with other APBs lying in intersecting planes becoming blocked or extending the area of the plane defect (see e.g., [62,63]). These processes dissipate energy even if the formed APB is destroyed by diffusion afterwards, since it is thermodynamically irreversible. Therefore the formation of these defects probably affect strain hardening as well (increasing the strain hardening exponent).

The symmetry and composition of the superlattice may, thus, have a strong impact in the morphology of the superdislocation and hence, on plastic deformation by slip. One of the present authors previously investigated the composition dependence of

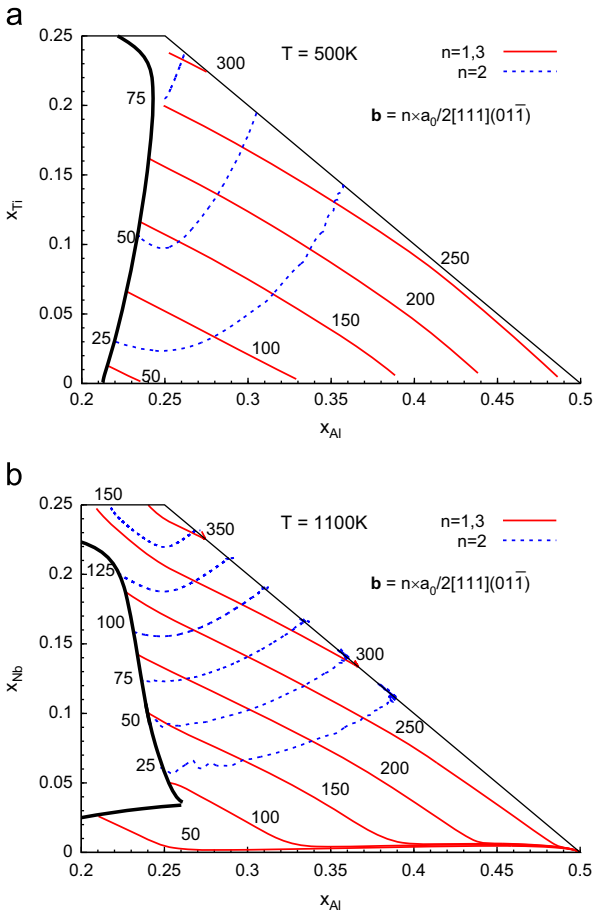

Fig. 11. Composition dependence of the mechanical APB energies, of APBs produced by dislocation slip in ternary aluminides: (a) Fe–Al–Ti system at $T=500$ K and (b) Fe–Al–Nb system at $T=1100$ K.

the energy of mechanical APBs formed by the slip of multiple $a_0/2\langle 1\ 1\ 1\rangle$ dislocations slipping in $\{0\ 1\ \overline{1}\}$ planes in Fe–Al alloys [42]. The results showed that large variations in the energy (of one order of magnitude) are expected to be observed in relatively small composition ranges, already in binary alloys.

Fig. 11 shows the composition dependence of mechanical APB energies in two partial isothermal sections of systems Fe–Al–Ti at $T=500$ K (Fig. 11a) and Fe–Al–Nb at $T=1100$ K (Fig. 11b). The temperatures were chosen such that the aluminide fields covers approximately the same composition range in both diagrams. The first obvious differences refers to the values of the energies in both systems. Both defects in Fe–Al–Nb are considerably more energetic in comparison with Fe–Al–Ti, as can be observed comparing the values, in spite of the lower temperature in the second calculation, which should result in larger order parameters. The form of the composition dependence, however, is also different in both systems. The APB energies grow smoothly towards the stoichiometric compositions in Fe–Al–Ti, while in Fe–Al–Nb both energies present a sharper maximum near the Fe_2AlNb composition. This shows not only that the conclusions of Ref. [42] referring to the binary aluminides are corroborated in the case of the ternary alloys (that is, the APB energies vary largely in relatively small composition ranges), but also that the behavior observed in different systems is peculiar of each system.

vThe present results (Fig. 11) show that the expected composition dependence of plastic deformation modes is also complex in ternary aluminides and that predicting this behavior in true multicomponent alloys is only viable within a proper multicomponent thermodynamic model, capable of dealing with the fine details of the crystal lattice symmetry.

4. Conclusions

In the present work, the metastable ordering equilibria in three ternary systems which are important for the development of iron aluminides are described. The different observed equilibria are experimentally observed (in systems Fe–Al–Ti and Fe–Al–Nb) or resemble features of experimental equilibria involving an iron aluminide matrix and more complex intermetallics (in the Fe–Al–Mo, the B2 phase is found in equilibrium with the A15 Mo_3Al phase [8,54]). These equilibria, in the iron-rich corner, are fundamentally defined by the equilibria in the binary Fe–M systems, which, with the sole exception of the existence of the B2 phase in the Fe–Ti system are all metastable.

This points out to very complex multiphase relations in the technical iron aluminides. As an example, the presence of a strong B2-FeTi phase could counteract the phase separation tendency in the Fe–Mo system, potentially increasing the Mo solubility in a quaternary system. The investigation of the metastable bcc ordering equilibria, therefore, assumes a crucial importance in aluminide alloy project.

The results shown here, however, are not only relevant to understand the phase relationships in ternary aluminides. The composition dependence of the thermodynamic force for diffusion and APB energies show complex non-linear dependencies, which are marked by discontinuities in second-order lines and sharp maxima in stoichiometric points or sections. This shows that the aluminide physical properties are also expected to be strongly affected by the different metastable equilibria, which require a proper thermodynamics modeling, unlikely to be reproduced by simpler solution models as the ones presently adopted in the CALPHAD method.

Acknowledgments

This work has been financially supported by the São Paulo State Research Funding Agency (FAPESP, São Paulo-SP, Brazil), by the Brazilian National Research Council (CNPq, Brasília-DF, Brazil), and by the Coordenação de Aperfeiçoamento de Pessoal de Nível Superior (CAPES, Brasília-DF, Brasil), and used some facilities at LCCA-USP and CENAPAD-UNICAMP, Brazil and at UNAC-FCNM-CI, Peru.

References

[1] A. Bahadur, Enhancement of high temperature strength and room temperature ductility of iron aluminides by alloying, Mater. Sci. Tech. 19 (2003) 1627–1634.
[2] M. Palm, Concepts derived from phase diagram studies for the strengthening of Fe–Al-based alloys, Intermetallics 13 (2005) 1286–1295.
[3] Z.-R. Zhang, W.-X. Liu, Mechanical properties of Fe_3Al-based alloys with addition of carbon, niobium and carbon, Mater. Sci. Eng. A 423 (2006) 343–349.
[4] C.G. McKamey, C.T. Liu, Chromium addition and environmental embrittlement in Fe_3Al, Scripta Met. Mater. 24 (1990) 2119–2122.
[5] R. Balasubramaniam, On the role of chromium in minimizing room temperature hydrogen embrittlement in iron aluminides, Scripta Mater. 34 (1996) 127–133.
[6] M. Palm, G. Inden, N. Thomas, The Fe–Al–Ti system, J. Phase Eq. 16 (1995) 209–222.
[7] I. Ohnuma, C. Schön, R. Kainuma, G. Inden, K. Ishida, Ordering and phase separation in the bcc phase of the Fe–Ti–Al system, Acta Mater. 46 (1998) 2083–2094.
[8] M. Eumann, M. Palm, G. Sauthoff, Phase equilibria in the Fe–Mo–Al system – part I: stability of the Laves phase Fe_2Mo and isothermal section at 800 °C, Intermetallics 16 (2008) 706–716.
[9] N. Sodré, P.G. Gonzales–Ormeño, H.M. Petrilli, C.G. Schön, Ab initio calculation of the Fe–Mo–Al (iron–molybdenum–aluminum) phase diagram: implications for the nature of the τ_2 phase, CALPHAD 33 (2009) 576–583.
[10] D.G. Morris, M.A. Muñoz-Morris, L.M. Requejo, C. Baudin, Strengthening at high temperatures by precipitates in Fe–Al–Nb alloys, Intermetallics 14 (2006) 1204–1207.
[11] D. De Fontaine, Cluster approach to order–disorder transformations in alloys, Solid State Phys. 47 (1994) 33–176.
[12] G. Ghosh, A. van de Walle, M. Asta, G.B. Olson, Phase stability of the Hf–Nb system: from first-principles to CALPHAD, CALPHAD 26 (2002) 491–511.
[13] C. Ravi, B.K. Panigrahi, M.C. Valkasumar, A. van de Walle, First-principles calculation of phase equilibrium of V–Nb, V–Ta, and Nb–Ta alloys, Phys. Rev. B 85 (2012) 054202.
[14] P. Blaha, K. Schwarz, G.K.H. Madsen, D. Kvasnicka, J. Luitz, WIEN2K, An augmented Plane Waves+Local Orbitals Program for Calculating Crystal Properties, (Karlheinz Schwarz, Tech. Universität Wien, Austria), ISBN 3950103112, 2001.
[15] N. Sodré, J.C. Garcia, L.V.C. Assali, P.G. Gonzales–Ormeño, H.M. Petrilli C.G. Schön, Intrinsic uncertainty on ab initio phase diagram and compound formation energy calculations: BCC Mo – Fe as a test case, Phys. Status Solidi B 250 (2012) 77–85.
[16] J.P. Perdew, K. Burke, M. Ernzernhof, Generalized gradient approximation made simple, Phys. Rev. Lett. 77 (1996) 3865.
[17] R. Kikuchi, A method of approximation for cooperative phenomena, Phys. Rev. 79 (1950) 718.
[18] R. Kikuchi, A theory of cooperative phenomena, Phys. Rev. 81 (1951) 988–1003.
[19] R. Kikuchi, CVM entropy algebra, Progr. Theor. Phys. Suppl. 115 (1994) 1–26.
[20] P.G. Gonzales-Ormeño, H.M. Petrilli, C.G. Schön, Ab initio calculation of the BCC Mo–Al (molybdenum–aluminum) phase diagram: implications for the nature of the ζ_2-MoAl phase, Scripta Mater. 53 (2005) 751–756.
[21] P.G. Gonzales-Ormeño, H.M. Petrilli, C.G. Schön, Ab initio calculation of the bcc Fe–Al phase diagram including magnetic interactions, Scripta Mater. 54 (2006) 1271–1276.
[22] C.G. Schön, G. Inden, CVM calculation of BCC phase diagrams using higher order cluster interactions, J. Chim. Phys. PCB 94 (1997) 1143–1151.
[23] R. McCormack, D. de Fontaine, C. Wolverton, G. Ceder, Nonempirical phase equilibria in the W–Mo–Cr system, Phys. Rev. B 51 (1995) 15808–15822.
[24] L.T.F. Eleno, C.G. Schön, J. Balun, G. Inden, Prototype calculations of *B2* miscibility gaps in ternary b.c.c. systems with strong ordering tendencies, Intermetallics 11 (2003) 1245–1252.
[25] K. Hack, The SGTE Casebook: Thermodynamics at Work, Materials Modelling Series, The Institute of Metals, London, UK, 1996.
[26] C.H.P. Lupis, Chemical Thermodynamics of Materials, North Holland New York, USA, 1983.
[27] R. Kikuchi, Superposition approximation and natural iteration calculation in cluster-variation method, J. Chem. Phys. 60 (1974) 1071–1080.
[28] T. Mohri, T. Morita, N. Kiyokane, H. Ishii, Theoretical investigation of lattice thermal vibration effects on phase equilibria within cluster variation method, J. Phase Equilib. 30 (2009) 553.
[29] G. Inden, C.G. Schön, Thermodynamic self-consistency issues related to the cluster variation method: the case of the bcc Cr–Fe (chromium–iron) system, CALPHAD 32 (2008) 661–669.

[30] V. Blum, A. Zunger, Structural complexity in binary bcc ground states: the case of bcc Mo–Ta, Phys. Rev. B 69 (2004) 020103. (R).
[31] P. Mohn, C. Persson, P. Blaha, K. Schwarz, P. Novák, H. Eschrig, Correlation induced paramagnetic ground state in FeAl, Phys. Rev. Lett. 87 (2001) 196401.
[32] F. Lechermann, F. Welsch, C. Elsässer, C. Ederer, M. Fähnle, J.M. Sanchez, B. Meyer, Density-functional study of Fe3Al: LSDA versus GGA, Phys. Rev. B 65 (2002) 132104.
[33] C.G. Schön, Order–disorder transformations and diffusion in ternary BCC alloys, J. Ph. Equilibria 22 (2001) 287–290.
[34] L. Tisza, Generalized Thermodynamics, M.I.T. Press, Cambridge-MA, USA, 1966.
[35] P.J. Shewmon, Diffusion in Solids, McGraw-Hill Book Co., New York, 1966.
[36] C.G. Schön, G. Inden, Concentration dependence of the excess specific heat capacity and of the thermodynamic factor for diffusion in FCC and BCC ordering systems, Acta Mater. 46 (1998) 4219–4231.
[37] J.W. Cahn, R. Kikuchi, Theory of domain walls in ordered structures—I. Properties at absolute zero, J. Phys. Chem. Solids 20 (1961) 94–109.
[38] P. Cenedese, R. Kikuchi, Scalar product method in statistical mechanics of boundary tension, J. de Physique I 7 (1996) 255–272.
[39] C.G. Schön, R. Kikuchi, Scalar-product cluster variation method layer formulation for the irregular tetrahedron cluster in bcc lattices, Phys. Rev. B 72 (2005) 094101.
[40] P.A. Flinn, Theory of deformation in superlattices, Trans. Metall. Soc. AIME 218 (1960) 145–154.
[41] C.G. Schön, R. Kikuchi, Antiphase boundary energy determination in superlattices based on the BCC lattice using the cluster variation method, Z. Metallk. 89 (1998) 868–878.
[42] C.G. Schön, R. Kikuchi, Cluster variation method for determining the energy of slip-induced anti-phase boundaries in BCC alloys, Theor. Appl. Frac. Mech. 35 (2001) 243–254.
[43] P.G. Gonzales-Ormeño, C.G. Schön, Electron theoretical investigation of the stability of the B2-TiFe compound, J. Alloys Comp. 470 (2008) 301–305.
[44] P.R. Alonso, P.H. Gargano, P.B. Bozzano, G.E. Ramirez–Caballero, P.B. Balbuena, G.H. Rubiolo, Combined ab initio and experimental study of A2+$L2_1$ cohjerent equilibria in Fe–Al–*X* (*X*=Ti, Nb, V), Intermetallics 19 (2011) 1157–1167.
[45] X. Yan, A. Grytsiv, P. Rogl, M. Palm, The Heusler phase $Ti_{25}(Fe_{50-x}, Ni_x)Al_{25}$ ($0 \le x \le 50$); structure and constitution, J. Phase Eq. Diff. 29 (2008) 500–508.
[46] L.T.F. Eleno, C.G. Schön, J. Balum, G. Inden, Experimental study and cluster variation modelling of the A2/B2 equilibria at the titanium-rich side of the Ti–Fe system, Z. Metallk. 95 (2004) 464–468.
[47] M. Palm, J. Lacaze, Assessment of the Fe–Ti–Al system, Intermetallics 14 (2006) 1291–1303.
[48] P.G. Gonzales-Ormeño, H.M. Petrilli, C.G. Schön, Ab initio calculations of the formation energies of BCC-based superlattices in the Fe–Al system, CALPHAD 26 (2002) 573–582.
[49] J.-O. Andersson, A thermodynamic evaluation of the Fe–Mo–C system, CALPHAD 12 (1988) 9–23.
[50] N. Saunders, Al–Mo (Aluminum–Molybdenum), in: T.B. Massalski (Ed.), Binary Alloy Phase Diagrams, vol. 1, ASM, Metals Park-OH, USA, 2nd ed., 1990, pp. 174–175.
[51] R. Kainuma, I. Ohnuma, K. Ishikawa, K. Ishida, Stability of B2 ordered phase in the Ti-rich portion of Ti–Al–Cr and Ti–Al–Fe ternary systems, Intermetallics 8 (2000) 869–875.
[52] I. Ohnuma, Y. Fijita, H. Mitsui, K. Ishikawa, R. Kainuma, K. Ishida, Phase equilibria in the Ti–Al binary system, Acta Mater. 48 (2000) 3113–3123.
[53] D.M. Cupid, O. Fabrichnaya, O. Rios, F. Ebrahimi, H.J. Seifert, Thermodynamic re-assesment of the Ti–Al–Nb system, Int. J. Mater. Res. 100 (2009) 218–233.
[54] M. Eumann, M. Palm, G. Sauthoff, Phase equilibria in the Fe–Mo–Al system—Part II: isothermal sections at 1000 and 1150 °C, Intermetallics 16 (2008) 834–845.
[55] L.T.F. Eleno, C.G. Schön, J. Balun, G. Inden, Prototype calculations of *B2* miscibility gaps in ternary b.c.c. systems with strong ordering tendencies, Intermetallics 11 (2003) 1245–1252.
[56] M. Palm, G. Inden, N. Thomas, The Fe–Al–Ti system, J. Phase Equilib. 16 (1995) 209–222.
[57] A. Grytsiv, P. Rogl, V. Pomjakushin, Structural transition with loss of symmetry in Ti–*M*–Al-based G-phases (*M* Fe, Co), Intermetallics 14 (2006) 784–791.
[58] K. Ishikawa, M. Ise, I. Ohnuma, R. Kainuma, K. Ishida, Phase equilibria and stability of the bcc aluminide in the Co–Cr–Al system, Berichte der Bunsengesellschaft für physikalische Chemie 102 (1998) 1–5.
[59] K. Ishikawa, R. Kainuma, I. Ohnuma, K. Aoki, K. Ishida, Phase stability of the X_{2AlTi} Heusler and B2-type intermetallic compounds, Acta Mater. 50 (2002) 2233–2243.
[60] N.S. Stoloff, Ordered alloys—physical metallurgy and structural applications, Int. Metals Rev. 29 (1984) 123–135.
[61] I. Baker, P.R. Munroe, Mechanical properties of FeAl, Int. Mater. Rev. 42 (1997) 181–205.
[62] F. Král, P. Schwander, G. Kostorz, Superdislocations and antiphase boundary energies in deformed Fe_3Al single crystals with chromium, Acta Mater. 45 (1997) 675–682.
[63] F. Král, Microstructure and mechanical properties of Fe_3Al with chromium, Dr. rer. nat., ETH-Zürich, Diss. ETH Nr. 11685, Zürich, Switzerland, 1996.